STRANGE AND CHARM MESONS AT FAIR*

L. Tolos[a], D. Cabrera[b], D. Gamermann[c], C. Garcia-Recio[d]
R. Molina[c], J. Nieves[c], E. Oset[c], A. Ramos[e]

[a]Theory Group. KVI. University of Groningen
Zernikelaan 25, 9747 AA Groningen, The Netherlands

[b]Departamento de Física Teórica II, Universidad Complutense
28040 Madrid, Spain

[c]Instituto de Física Corpuscular (centro mixto CSIC-UV)
Institutos de Investigación de Paterna, Aptdo. 22085, 46071, Valencia, Spain

[d] Departamento de Física Atómica, Molecular y Nuclear, Universidad de Granada
18071 Granada, Spain

[e]Departament d'Estructura i Constituents de la Matèria, Universitat de Barcelona
Diagonal 647, 08028 Barcelona, Spain

We study the properties of strange and charm mesons in hot and dense matter within a self-consistent coupled-channel approach for the experimental conditions of density and temperature expected for the CBM experiment at FAIR/GSI. The in-medium solution at finite temperature accounts for Pauli blocking effects, mean-field binding of all the baryons involved, and meson self-energies. We analyse the behaviour in this hot and dense environment of dynamically-generated baryonic resonances together with the evolution with density and temperature of the strange and open-charm meson spectral functions. We test the spectral functions for strange mesons using energy-weighted sum rules and finally discuss the implications of the properties of charm mesons on the $D_{s0}(2317)$ and the predicted $X(3700)$ scalar resonances.

PACS numbers: 11.10.St, 12.38.Lg, 14.20.Lq, 14.40.Lb

1. Introduction

Over the last decades strangeness has been a matter of extensive study in connection to exotic atoms [1] as well as heavy-ion collisions at SIS/GSI energies [2]. Phenomenology of antikaonic atoms shows that the $\bar{K}$ feels an

---

* Presented at the XXXI Mazurian Lakes Conference on Physics, Piaski, Poland, August 30–September 6, 2009.

attractive potential at low densities. This attraction results from the modified s-wave $\Lambda(1405)$ resonance in the medium due to Pauli blocking effects [3] together with the self-consistent consideration of the $\bar{K}$ self-energy [4] and the inclusion of self-energies of the mesons and baryons in the intermediate states [5]. Attraction of the order of -50 MeV at normal nuclear matter density, $\rho_0 = 0.17\,\mathrm{fm}^{-3}$, is obtained by different approaches, such as unitarized theories in coupled channels based on meson-exchange models [6] or chiral dynamics [5]. Higher-partial waves beyond the s-wave contribution have been also studied [7–9] as they become relevant for heavy-ion collisions at beam energies below $2A\,\mathrm{GeV}$ [2].

Also the charm degree of freedom is a recent topic of analysis in heavy-ion experiments. The CBM experiment of the future FAIR project at GSI will investigate highly compressed dense matter in nuclear collisions with a beam energy range between 10 and $40\,\mathrm{GeV}/u$. An important part of the hadron physics project is devoted to extend the SIS/GSI program for the in-medium modification of hadrons to the heavy quark sector providing a first insight into charm–nucleus interaction. Thus, the possible modifications of the properties of open and hidden charm mesons in a hot and dense environment are matter of recent studies.

The in-medium modification of the open charm mesons (D and $\bar{D}$) may help to explain the J/Ψ suppression in a hadronic environment as well as the possible formation of D-mesic nuclei. Moreover, changes in the properties of open charm mesons will affect the renormalisation of charm and hidden charm scalar meson resonances in nuclear matter, providing information about their nature, whether they are $q\bar{q}$ states, molecules, mixtures of $q\bar{q}$ with meson–meson components, or dynamically generated resonances resulting from the interaction of two pseudoscalars.

In the present article, we present a study of the properties of strange and charm mesons in hot and dense matter within a self-consistent approach in coupled channels for the conditions expected at CBM/FAIR. We analyse the behaviour of dynamically generated baryonic resonances as well as the strange and charm meson spectral functions in this hot and dense medium. We then test our results for strange mesons using energy-weighted sum rules and analyse the effect of the self-energy of D mesons on dynamically-generated charm and hidden charm scalar resonances.

2. Strange and charm mesons in hot and dense matter

The self-energy and, hence, the spectral function at finite temperature for strange ($\bar{K}$ and K) and charm (D and $\bar{D}$) mesons are obtained following a self-consistent coupled-channel procedure. We start by solving the Bethe–Salpeter equation in coupled channels or T-matrix (T) taking, as bare

interaction, a transition potential coming from effective Lagrangians. Details about this bare interaction for strange and charm mesons are given in the next sections. The self-energy is then obtained summing the transition amplitude T for the different isospins over the nucleon Fermi distribution at a given temperature, $n(\vec{q}, T)$, as

$$\Pi(q_0, \vec{q}, T) = \int \frac{d^3p}{(2\pi)^3} \, n(\vec{p}, T) \left[T^{(I=0)} \left(P_0, \vec{P}, T \right) + 3T^{(I=1)} \left(P_0, \vec{P}, T \right) \right], \quad (1)$$

where $P_0 = q_0 + E_N(\vec{p}, T)$ and $\vec{P} = \vec{q} + \vec{p}$ are the total energy and momentum of the meson–nucleon pair in the nuclear matter rest frame, and $(q_0, \vec{q})$ and $(E_N, \vec{p})$ stand for the energy and momentum of the meson and nucleon, respectively, also in this frame. The self-energy must be determined self-consistently since it is obtained from the in-medium amplitude T which contains the meson–baryon loop function, and this last quantity itself is a function of the self-energy. The meson spectral function then reads

$$S(q_0, \vec{q}, T) = -\frac{1}{\pi} \frac{\mathrm{Im}\,\Pi(q_0, \vec{q}, T)}{|q_0^2 - \vec{q}^2 - m^2 - \Pi(q_0, \vec{q}, T)|^2} . \quad (2)$$

In this paper we analyse the properties of strange and charm mesons for the experimental conditions of density and temperature expected at CBM. The range of validity of our model allows us to reach temperatures of the order of hundred MeV while densities above two–three times nuclear matter density may require models beyond the T-matrix approach.

3. Strange mesons

The kaon self-energies in symmetric nuclear matter at finite temperature are obtained from the in-medium kaon–nucleon interaction within a chiral unitary approach which incorporates the s- and p-wave contributions [9].

At tree level, the s-wave amplitude arises from the Weinberg–Tomozawa (WT) term of the chiral Lagrangian. Unitarisation in coupled channels is imposed by solving the Bethe–Salpeter equation with on-shell amplitudes and a cutoff regularisation. The unitarized $\bar{K}N$ amplitude generates dynamically the $\Lambda(1405)$ resonance in the $I = 0$ channel and provides a satisfactory description of low-energy scattering observables. The in-medium solution of the s-wave amplitude accounts for Pauli-blocking effects, mean-field binding on the nucleons and hyperons via a σ–ω model, and the dressing of the pion and kaon propagators via their corresponding self-energies in a self-consistent manner. The model includes, in addition, a p-wave contribution to the self-energy from hyperon–hole (Yh) excitations, where Y stands for Λ, Σ and Σ^* components.

The upper part of Fig. 1 shows the real and imaginary parts of the $\bar{K}$ self-energy together with the $\bar{K}$ spectral function as a function of the $\bar{K}$ energy at $\rho_0 = 0.17 \text{ fm}^{-3}$ for two different momenta, $q = 0 \text{ MeV}/c$ (left column) and $q = 450 \text{ MeV}/c$ (right column). The different curves correspond to $T = 0$ and $T = 100 \text{ MeV}$ including the s-wave and the $(s+p)$-wave contributions. The self-energy is dominated by the s-wave dynamics and the p-wave contributions from ΛN^{-1}, ΣN^{-1} and $\Sigma^* N^{-1}$ excitations become evident at a finite momentum of $q = 450 \text{ MeV}/c$. The effect of these subthreshold excitations is repulsive at the $\bar{K}N$ threshold. This repulsion together with the strength below threshold can be easily seen in the spectral function at finite momentum (third row). At finite momentum the quasi-particle peak moves to higher energies while the spectral function falls off slowly on the left-hand side. Temperature results in a softening of the real and imaginary
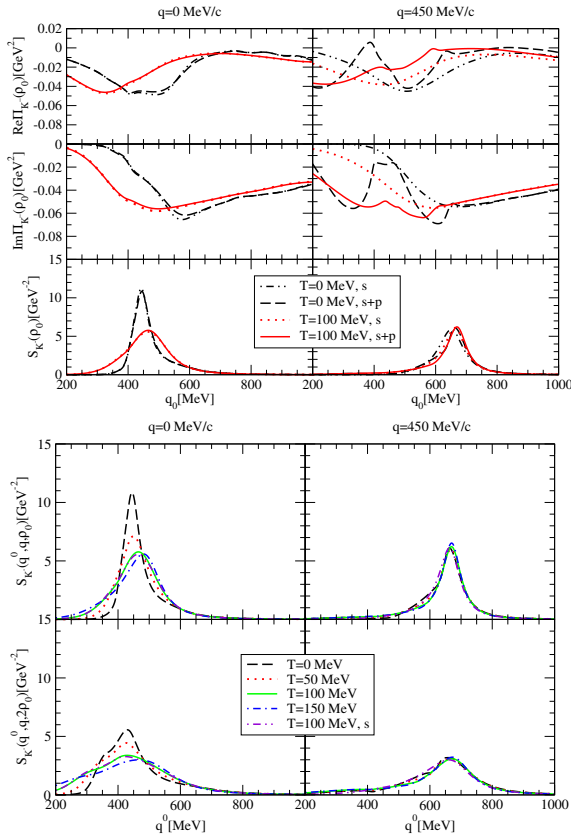

Fig. 1. Top: $\bar{K}$ self-energy and spectral function for $\rho = \rho_0$, $T = 0, 100 \text{ MeV}$ and two momenta showing the partial wave decomposition. Bottom: Evolution of the $\bar{K}$ spectral function with temperature for two momenta and two densities: ρ_0 (upper panels) and $2\rho_0$ (lower panels).

part of the self-energy as the Fermi surface is smeared out. The peak of the spectral function moves closer to the free position while the spectral function extends over a wider range of energies.

The evolution with density and temperature of the $\bar{K}$ spectral function is depicted on the bottom part of Fig. 1. The spectral function shows a strong mixing between the quasi-particle peak and the $\Lambda(1405)N^{-1}$ and YN^{-1} excitations. As we have seen before, the effect of the p-wave YN^{-1} subthreshold excitations is repulsive for the $\bar{K}$ potential, compensating in part the attraction from the s-wave $\bar{K}N$ interaction. Temperature softens the p-wave contributions to the spectral function at the quasi-particle energy. Moreover, together with the s-wave mechanisms, the p-wave self-energy provides a low-energy tail which spreads the spectral function considerably. Increasing the density dilutes the spectral function even further.

3.1. Energy weighted sum rules

The hadron propagator or single particle Green's function has well defined analytical properties that impose some constraints on the many-body formalism as well as the interaction model. An excellent tool to test the quality of our model for hadrons in medium is provided by the energy-weighted sum rules (EWSRs) of the single-particle spectral functions. The EWSRs are obtained from matching the Dyson form of the meson propagator with its spectral Lehmann representation at low and high energies [10]. The first EWSRs in the high-energy limit expansion, $m_0^{(\mp)}$, together with the zero energy one, m_{-1}, are given by

$$m_{-1}: \int_0^\infty d\omega \frac{1}{\omega} \left[S_{\bar{K}}(\omega, \vec{q}; \rho, T) + S_K(\omega, \vec{q}; \rho, T) \right] = \frac{1}{\omega_{\bar{K}}^2(\vec{q}) + \Pi_{\bar{K}}(0, \vec{q}; \rho, T)} \, , \quad (3)$$

$$m_0^{(\mp)}: \int_0^\infty d\omega \left[S_{\bar{K}}(\omega, \vec{q} \, \rho, T) - S_K(\omega, \vec{q}; \rho, T) \right] = 0 \, ,$$

$$\int_0^\infty d\omega \, \omega \left[S_{\bar{K}}(\omega, \vec{q}; \rho, T) + S_K(\omega, \vec{q}; \rho, T) \right] = 1 \, . \quad (4)$$

The sum rules for the antikaon propagator are shown in Fig. 2 as a function of the upper integral limit in the case of $\rho = \rho_0$, $T = 0$ MeV and $q = 150$ MeV$/c$. The contributions from $\bar{K}$ and K to the l.h.s. of the sum rule are depicted separately. The $\bar{K}$ and K spectral functions are also shown for reference in arbitrary units. Note that saturation is progressively shifted to higher energies as we examine sum rules involving higher order weights in energy.
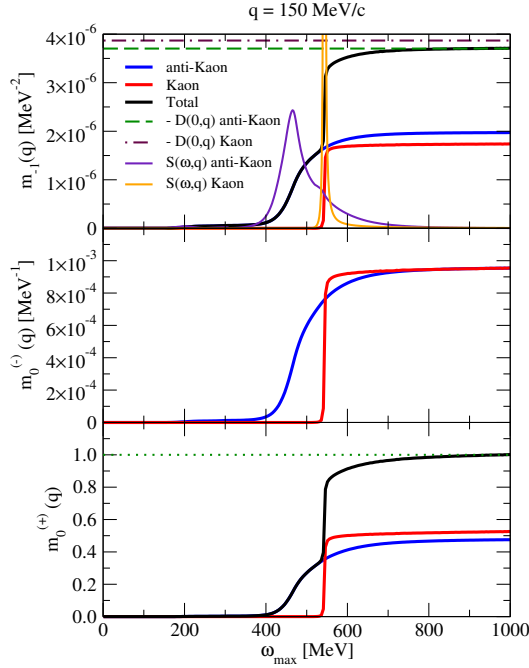
Fig. 2. m_{-1}, $m_0^{(-)}$ and $m_0^{(+)}$ sum rules for the K and $\bar{K}$ spectral functions at $q = 150\,\mathrm{MeV}/c$, $\rho = \rho_0$ and $T = 0\,\mathrm{MeV}$. The $\bar{K}$ and K spectral functions are also displayed for reference in arbitrary units.

The l.h.s. of the m_{-1} sum rule (upper panel) converges properly and saturates a few hundred MeV beyond the quasiparticle peak, following the behaviour of the $\bar{K}$ and K spectral functions. We have also plotted in Fig. 2 the r.h.s. of the m_{-1} sum rule both for the antikaon and kaon, namely their off-shell propagators evaluated at zero energy (modulo a minus sign). The difference between both values reflects the violation of crossing symmetry present in the chiral model employed for the kaon and antikaon self-energies as we neglect the explicit exchange of a meson–baryon pair in a t-channel configuration. However, we may still expect the saturated value of the l.h.s. of the m_{-1} sum-rule to provide a constraint for the value of the zero-mode propagator appearing on the r.h.s., because the most of the strength sets in at energies of the order of the meson mass, where the neglected terms of the $K(\bar{K})N$ amplitudes are irrelevant.

The $m_0^{(-)}$ sum rule shows that the areas subtended by the K and $\bar{K}$ spectral functions should coincide. This is indeed the case for the calculation considered here, as can be seen in the middle panel of Fig. 2. The fulfillment of this sum rule is, however, far from trivial. We recall that

whereas one expects the $\bar{K}$ and K spectral functions to be related by the retardation property, $S_{\bar{K}}(-\omega) = -S_K(\omega)$, the actual calculation of the meson self-energies is done exclusively for positive meson energies.

The $m_0^{(+)}$ sum rule saturates to one independently of the meson momentum, nuclear density or temperature, thus posing a strong constraint on the accuracy of the calculations. The lower panel in Fig. 2 shows that the K and $\bar{K}$ spectral functions fulfill this sum rule to a high precision.

We have also tested those sum rules for higher momenta and temperature. As the meson momentum is increased, the saturation of the integral part of the sum rules is progressively shifted to higher energies, following the strength of the spectral distribution. At finite temperature the $\bar{K}$ spectral function spreads considerably [9], and in particular acquires a sizable low energy tail from smearing of the Fermi surface, which contributes substantially to the l.h.s. of the sum rule below the quasi-particle peak. The K contribution also softens at finite temperature and increasing momenta, as the K in-medium decay width is driven by the KN thermal phase space.

4. Charm mesons

The properties of charm mesons is a topic of recent analysis and lot of effort is being invested in constructing effective models for the meson–baryon interaction in the charm sector. In this section we present two different approaches to this effective meson–baryon interaction. We then discuss possible experimental scenarios where the charm meson properties can be tested, such as scalar resonances in nuclear matter.

4.1. SU(4) t-vector meson exchange models

The D and $\bar{D}$ meson spectral functions are obtained from the multichannel Bethe–Salpeter equation taking, as bare interaction, a type of broken $SU(4)$ s-wave WT interaction supplemented by an attractive isoscalar–scalar term and using a cutoff regularisation scheme. This cutoff is fixed by the position and the width of the $I = 0$ $\Lambda_c(2593)$ resonance. As a result, a new resonance in $I = 1$ channel $\Sigma_c(2880)$ is generated [11]. The in-medium solution at finite temperature incorporates, as well, Pauli blocking effects, baryon mean-field bindings and π and D meson self-energies [12].

The $I = 0$ $\tilde{\Lambda}_c$ and $I = 1$ $\tilde{\Sigma}_c$ resonances in hot dense matter are shown in the l.h.s. of Fig. 3 for two different self-consistent calculations: *(i)* including only the self-consistent dressing of the D meson, *(ii)* including mean-field binding on baryons and the pion self-energy. Medium effects at $T = 0$ lower the position of the $\tilde{\Lambda}_c$ and $\tilde{\Sigma}_c$ with respect to their free values. Their width values, which increase due to $\tilde{Y}_c(= \tilde{\Lambda}_c, \tilde{\Sigma}_c)N \to \pi N \Lambda_c, \pi N \Sigma_c$ processes,
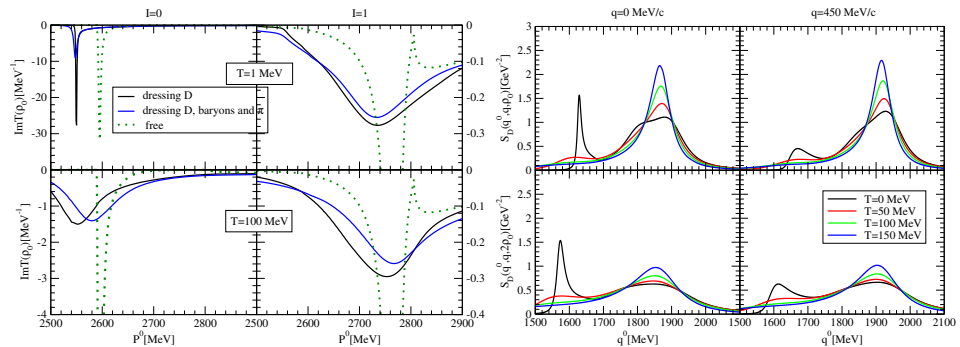
Fig. 3. Left: $\tilde{\Lambda}_c$ and $\tilde{\Sigma}_c$ resonances. Right: The D meson spectral function for different temperatures and two densities: ρ_0 (upper panel) and $2\rho_0$ (lower panel).

differ according to the phase space available. The pion dressing induces a small effect in the resonances because of charm-exchange channels being suppressed. Finite temperature results in the reduction of the Pauli blocking due to the smearing of the Fermi surface. Both resonances move up in energy closer to their free position while they are smoothed out, as in [7].

In the r.h.s. of Fig. 3 we display the evolution with density and temperature of the D meson spectral function for *(ii)*. At $T = 0$ the spectral function presents two peaks: $\tilde{\Lambda}_c N^{-1}$ excitation at a lower energy whereas the second one at higher energy is the quasi(D)-particle peak mixed with the $\tilde{\Sigma}_c N^{-1}$ state. Those structures dilute with increasing temperature while the quasiparticle peak gets closer to its free value becoming narrower, as the self-energy receives contributions from higher momentum DN pairs where the interaction is weaker. Finite density results in a broadening of the spectral function because of the increased decay and collisional phase space. Similar effects were observed previously for the $\bar{K}$ in hot dense nuclear matter [9].

4.2. SU(8) scheme with heavy-quark symmetry

Heavy-quark symmetry (HQS) is a proper QCD spin-flavor symmetry that appears when the quark masses, such as the charm mass, become larger than the typical confinement scale. As a consequence of this symmetry, the spin interactions vanish for infinitely massive quarks. Thus, heavy hadrons come in doublets (if the spin of the light degrees of freedom is not zero), which are degenerated in the infinite quark-mass limit. And this is the case for the D meson and its vector partner, the D^* meson.

Therefore, we calculate the self-energy and, hence, the spectral function of the D and D^* mesons in nuclear matter simultaneously from a self-consistent calculation in coupled channels. To incorporate HQS to the

meson–baryon interaction we extend the WT meson–baryon Lagrangian to the SU(8) spin-flavor symmetry group as we include pseudoscalars and vector mesons together with $J = 1/2^+$ and $J = 3/2^+$ baryons [13], following the steps for SU(6) of Ref. [14]. However, the SU(8) spin-flavor is strongly broken in nature. On one hand, we take into account mass breaking effects by adopting the physical hadron masses in the tree level interactions and in the evaluation of the kinematical thresholds of different channels, as done in SU(4) models. On the other hand, we consider the difference between the weak non-charmed and charmed pseudoscalar and vector meson decay constants. We also improve on the regularisation scheme in nuclear matter going beyond the usual cutoff scheme [15].

The SU(8) model generates a wider spectrum of resonances with charm $C = 1$ and strangeness $S = 0$ content compared to the previous SU(4) models, as seen in the top panel of Fig. 4. While the parameters of both SU(4)
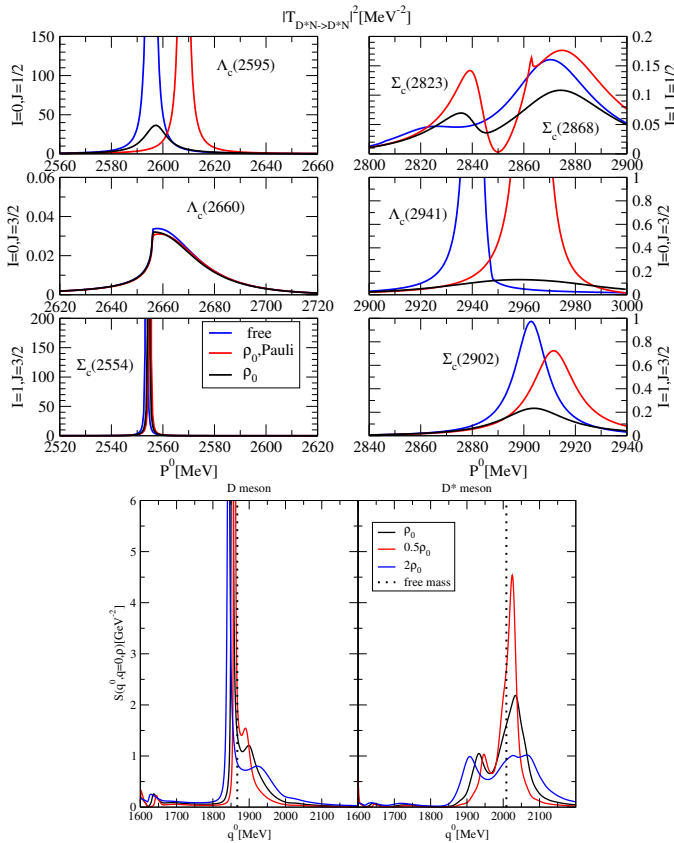

Fig. 4. Top: Dynamically-generated charmed baryonic resonances in nuclear matter. Bottom: D and D^* spectral functions in nuclear matter at $q = 0\,\mathrm{MeV}/c$.

and SU(8) models are fixed by the ($I = 0$, $J = 1/2$) $\Lambda_c(2595)$ resonance, the incorporation of vectors mesons in the SU(8) scheme generates naturally $J = 3/2$ resonances, such as $\Lambda_c(2660)$, $\Lambda_c(2941)$, $\Sigma_c(2554)$ and $\Sigma_c(2902)$, which might be identified experimentally [16]. New resonances are also produced for $J = 1/2$, as $\Sigma_c(2823)$ and $\Sigma_c(2868)$, while others are not observed in SU(4) models due to the different symmetry breaking pattern used in both models. The modifications of the mass and width of these resonances in the nuclear medium will strongly depend on the coupling to channels with D, D^* and nucleon content. Moreover, the resonances close to the DN or D^*N thresholds change their properties more evidently as compared to those far offshell. The improvement in the regularisation/renormalisation procedure of the intermediate propagators in the nuclear medium beyond the usual cutoff method has also an important effect on the in-medium changes of the dynamically-generated resonances, in particular, for those lying far offshell from their dominant channel, as the case of the $\Lambda_c(2595)$.

In the bottom panel of Fig. 4 we also display the D and D^* spectral functions, which show then a rich spectrum of resonant-hole states. The D meson quasiparticle peak mixes strongly with $\Sigma_c(2823)N^{-1}$ and $\Sigma_c(2868)N^{-1}$ states while the $\Lambda_c(2595)N^{-1}$ is clearly visible in the low-energy tail. The D^* spectral function incorporates the $J = 3/2$ resonances, and the quasiparticle peak fully mixes with $\Sigma_c(2902)N^{-1}$ and $\Lambda_c(2941)N^{-1}$. As density increases, these Y_cN^{-1} modes tend to smear out and the spectral functions broaden as the collisional and absorption processes increase.

4.3. Charm and hidden charm resonances in nuclear matter

The nature of a resonance, whether it has the usual $q\bar{q}/qqq$ structure or is better described as being dynamically generated, is an active matter of research, in particular, for scalar resonances. The excitation mechanisms in the nucleus together with the properties of those particles can be extracted studying their renormalized properties in nuclear matter.

We study the charmed resonance $D_{s0}(2317)$ [17,18] together with a hidden charm scalar meson, $X(3700)$, predicted in [18], which might have been observed by the Belle Collaboration [19] via the reanalysis of [20]. Those resonances are generated dynamically solving the coupled-channel Bethe–Salpeter equation for two pseudoscalars [21]. The kernel is derived from a SU(4) extension of the SU(3) chiral Lagrangian used to generate scalar resonances in the light sector. The SU(4) symmetry is, however, strongly broken, mostly due to the explicit consideration of the masses of the vector mesons exchanged between pseudoscalars [18].

The analysis of the transition amplitude close to each resonance for the different coupled channels gives us information about the coupling of the resonance to a particular channel. The $D_{s0}(2317)$ mainly couples to the

DK system, while the hidden charm state $X(3700)$ couples most strongly to $D\bar{D}$. Therefore, any change in the D meson properties in nuclear matter will have an important effect on these resonances. Those modifications are given by the D meson self-energy, as discussed in Sec. 4.1, but supplemented by the p-wave self-energy through the corresponding Y_cN^{-1} excitations [21].

In Fig. 5, the resonances $D_{s0}(2317)$ and $X(3700)$ are shown via the squared transition amplitude for the corresponding dominant channel. The $D_{s0}(2317)$ and $X(3700)$ resonances, which have a zero and small width develop widths of the order of 100 and 200 MeV at normal nuclear matter density, respectively. The origin can be traced back to the opening of new many-body decay channels, as the D meson gets absorbed in the nuclear medium via DN and DNN inelastic reactions. In our model, we do not extract any clear conclusion for the mass shift. We suggest to look at transparency ratios since they are very sensitive to the in-medium widths.
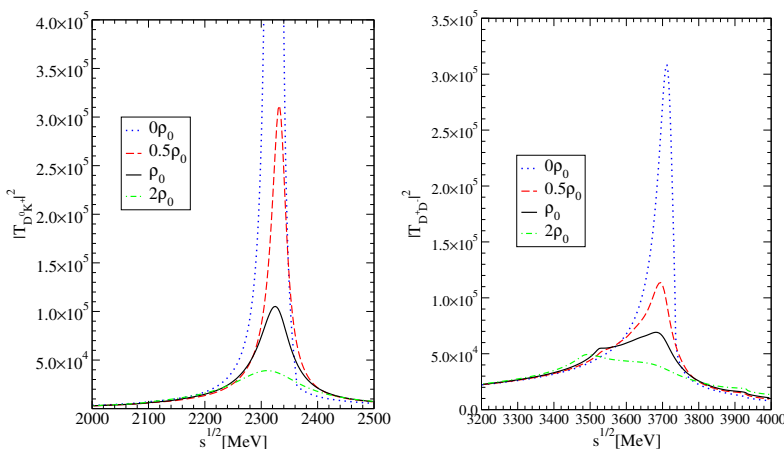

Fig. 5. $D_{s0}(2317)$ (left) and $X(3700)$ (right) resonances.

5. Conclusions and outlook

We have studied the properties of strange and charm mesons in hot and dense matter within a self-consistent coupled-channel approach. The in-medium solution at finite temperature accounts for Pauli blocking effects, mean-field binding on all the baryons involved, and meson self-energies. We have analyzed the behaviour in this hot and dense environment of dynamically-generated baryonic resonances together with the evolution with density and temperature of the strange and open-charm meson spectral functions. The spectral function for $\bar{K}$ and D mesons dilutes with increasing temperature and density while the quasiparticle peak moves closer to the free position. The spectral function for strange mesons is also tested using

energy-weighted sum rules and we found that the sum rules for the lower energy weights are fulfilled satisfactorily. We have finally discussed the implications of the properties of charm mesons on the $D_{s0}(2317)$ and the predicted $X(3700)$. We suggest to look at transparency ratios to investigate the changes in width of those resonances in nuclear matter.

REFERENCES

[1] E. Friedman, A. Gal, *Phys. Rep.* **452**, 89 (2007).
[2] C. Fuchs, *Prog. Part. Nucl. Phys.* **56**, 1 (2006).
[3] V. Koch, *Phys. Lett.* **B337**, 7 (1994).
[4] M. Lutz, *Phys. Lett.* **B426**, 12 (1998).
[5] A. Ramos, E. Oset, *Nucl. Phys.* **A671**, 481 (2000).
[6] L. Tolos, A. Ramos, A. Polls, T.T.S. Kuo, *Nucl. Phys.* **A690**, 547 (2001); L. Tolos, A. Ramos, A. Polls, *Phys. Rev.* **C65**, 054907 (2002).
[7] L. Tolos, A. Ramos, E. Oset, *Phys. Rev.* **C74**, 015203 (2006).
[8] M.F.M. Lutz, C.L. Korpa, M. Moller, *Nucl. Phys.* **A808**, 124 (2008).
[9] L. Tolos, D. Cabrera, A. Ramos, *Phys. Rev.* **C78**, 045205 (2008).
[10] D. Cabrera, A. Polls, A. Ramos, L. Tolos, *Phys. Rev.* **C80**, 045201 (2009).
[11] M.F.M. Lutz, C.L. Korpa, *Phys. Lett.* **B633**, 43 (2006); T. Mizutani, A. Ramos, *Phys. Rev.* **C74**, 065201 (2006).
[12] L. Tolos, A. Ramos, T. Mizutani, *Phys. Rev.* **C77**, 015207 (2008).
[13] C. Garcia-Recio, V.K. Magas, T. Mizutani, J. Nieves, A. Ramos, L.L. Salcedo, L. Tolos, *Phys. Rev.* **D79**, 054004 (2009).
[14] C. Garcia-Recio, J. Nieves, L.L. Salcedo, *Phys. Rev.* **D74**, 034025 (2006).
[15] L. Tolos, C. Garcia-Recio, J. Nieves, *Phys. Rev.* **C80**, 065202 (2009).
[16] [Particle Data Group] C. Amsler *et al.*, *Phys. Lett.* **B667**, 1 (2008).
[17] E.E. Kolomeitsev, M.F.M. Lutz, *Phys. Lett.* **B582**, 39 (2004); F.K. Guo, P.N. Shen, H.C. Chiang, R.G. Ping, *Phys. Lett.* **B641**, 278 (2006).
[18] D. Gamermann, E. Oset, D. Strottman, M.J. Vicente Vacas, *Phys. Rev.* **D76**, 074016 (2007).
[19] [Belle Collaboration] K. Abe *et al.*, *Phys. Rev. Lett.* **100**, 202001 (2008).
[20] D. Gamermann, E. Oset, *Eur. Phys. J.* **A36**, 189 (2008).
[21] R. Molina, D. Gamermann, E. Oset, L. Tolos, *Eur. Phys. J.* **A42**, 31 (2009).